ELSEVIER

Spectrochimica Acta Part B 57 (2002) 919–928

SPECTROCHIMICA ACTA PART B

www.elsevier.com/locate/sab

L-shell transition rates for Ba, Ta, W, Pt, Pb and Bi using electron microprobe

J. Trincavelli[a,b,*], G. Castellano[a], R. Bonetto[b,c]

[a]*Facultad de Matemática, Astronomía y Física, Universidad Nacional de Córdoba. Ciudad Universitaria, (5000) Córdoba, Argentina*

[b]*Consejo Nacional de Investigaciones Científicas y Técnicas de la República Argentina*

[c]*Centro de Investigación y Desarrollo de Procesos Catalíticos, CONICET-UNLP. Calle 47 N° 257-CC 59, (1900) La Plata, Argentina*

Received 5 December 2001; accepted 21 February 2002

Abstract

L-shell transition rates for several elements are obtained by means of a method for refining atomic and experimental parameters in electron probe microanalysis. An analytical function is used to account for the bremsstrahlung, characteristic peaks and detection artifacts from an irradiated material. The refinement procedure consists of minimizing the differences between the experimental X-ray spectrum and that predicted by means of the function proposed. In this work, the spectra considered were recorded with an energy dispersive system. The procedure is applied to Ta, W, Pt, Pb and Bi pure samples and a $BaSO_4$ sample. More than ten transitions are studied for each element. The results obtained are in agreement with data given in the literature. Finally, the optimization procedure is applied to the refinement of mass concentrations in a sample in which L-lines are strongly overlapped with K lines.

Keywords: Electron probe microanalyzer; Inner-shell ionization; Intensity ratio; Mathematical modeling; Standardless analysis

1. Introduction

The relative transition probabilities corresponding to decays to L-subshells are atomic parameters, which are very useful in the scope of different spectroscopic techniques. Several publications were devoted to the theoretical prediction [1], tabulation [2] and experimental determinations [3] of intensity ratios involving L-subshells. The reason why special attention has been paid to L transition rates is mainly because reliable experimental values can be used as a straight test for theoretical atomic models. In addition, the adequate knowledge of transition rates may improve the analyses by spectroscopic techniques based on X-ray emission, since the peak overlaps between different lines of neighboring elements are frequently a problem for the analyst.

The ratio between intensities corresponding to decays involving different final subshells may

*Corresponding author. Tel.: +54-351-4334-051; fax: +54-351-4334-054.

E-mail address: jorge@quechua.fis.uncor.edu (J. Trincavelli).

0584-8547/02/$ - see front matter
PII: S0584-8547(02)00022-8

depend on experimental conditions such as beam energy, since ionization cross-sections are different functions of energy for each considered subshell. Therefore, line intensity ratios must be considered separately according to the final subshell involved. These intensity ratios corrected for absorption in the sample and for efficiency losses in the detector are the atomic transition rates sought in the present work. In fact, these transition rates could slightly depend on the incidence energy if the ejected electron is slow enough to interact with the decaying atom during its removal. However, in order to measure such effect, specific experiments should be performed at very low over-voltages.

When determining these ratios experimentally, a number of problems arise, since spectral deconvolution and correction for absorption may be complicated. Therefore, spectra with good statistics may not be enough for determining accurate intensity ratios, especially for energy-dispersive detection systems (EDS). In the present work, the problem of characterizing L-shell line ratios was investigated by means of a method of parameter refinement. This methodology, which involves regions of the whole spectrum, is a widespread technique in powder X-ray diffraction, and has extensively been used in crystalline structural analysis [4–7]. Recently, the method of parameter optimization has been extended to electron probe microanalysis and X-ray fluorescence by means of the codes POEMA [8,9] and PRAXIS [10], respectively.

The method consists of performing minimization of quadratic differences between experimental and predicted values for different regions of the spectrum by means of an iterative process. If I_i and $\tilde{I}_i$ denote, respectively, the experimental and calculated intensities measured for the energy E_i, the quantity to be minimized can be written as:

$$\chi^2 = \frac{1}{N-P}\sum_i \frac{(\tilde{I}_i - I_i)^2}{I_i} \tag{1}$$

where the summation runs over all N data points and P is the number of parameters adjusted. Thus, χ^2 will depend on the parameters to optimize through the expressions chosen for $\tilde{I}_i$.

The functions used for the predicted spectrum are based on semiempirical analytical expressions for characteristic lines and bremsstrahlung emission, taking also into account detection artifacts. Thus, the spectrum is predicted as a complex function, which involves several magnitudes related to production, attenuation and detection of X-rays, sample composition, experimental parameters, etc. Depending on the particular situation, certain variables may be known a priori, so that they can be fixed allowing the others to move.

In order to obtain refined values for the magnitudes of interest, a numerical iterative procedure is performed, starting from certain initial guesses. These starting values must be quite close to the correct values in order to reduce the risk of falling in local minima. An alternative way to overcome this problem is to begin with different estimates and check that the same minimum is achieved.

In the case of the present work, the parameters sought are the radiative atomic transition rates involving decays to L-subshells. In addition, an application is shown for mass concentration refinement using the values for L-transition rates obtained for Ba.

2. Description of the method

In order to perform the optimization routine, a realistic description of the spectra acquired in EPMA and a good numerical procedure to minimize the differences between experimental and calculated spectra are necessary. This is accomplished by the code POEMA (an acronym for Parameter Optimization in Electron Microprobe Analysis) as detailed in this section.

The continuum spectrum corresponding to the emission of bremsstrahlung B is described by means of an analytical function of photon energy E, mean atomic number $\bar{Z}$ and incident energy E_o of the electron beam impinging on the sample [11]:

$$B = \alpha\sqrt{\bar{Z}}\frac{E_o - E}{E}\left[-54.86 - 1.072E + 0.2835E_o + 30.4\ln\bar{Z} + \frac{875}{\bar{Z}^2 E_o^{0.08}}\right]\mathbf{A}_B R \in \tag{2}$$

where α is proportional to the number of incident electrons and to the fraction of solid angle subtended by the detector, $\mathbf{A}_B$ corrects for X-ray absorption, R takes into account intensity losses due to electron backscattering and $\in$ is the detector efficiency at energy E.

The detected characteristic intensity $P_{j,q}$ of the line q from element j in the sample can be written as [12]:

$$P_{j,q} = \gamma C_j (\mathbf{ZAF})_{j,q} Q_{j,q} \omega_{j,q} f_{j,q} \in_{j,q} \quad (3)$$

where γ is proportional to the number of incident electrons and to the fraction of solid angle subtended by the detector; C_j is the mass concentration for element j; **Z**, **A** and **F** indicate the atomic number, absorption and fluorescence matrix corrections, respectively, $Q_{j,q}$ is the ionization cross-section for element j at the energy E_o, $\omega_{j,q}$ is the fluorescence yield for the considered atomic subshell and $f_{j,q}$ is the transition rate related to the observed line q. It is worth emphasizing that, along this work, each of these transition rates represents the probability for one specific decay normalized to the total probability for radiative decays corresponding to a particular subshell. A description of the interaction between electrons and matter involving an ionization distribution function $\phi(pz)$ with mass depth pz was considered for this work to account for both **Z** and **A** correction factors. Packwood and Brown's [13] description of $\phi(pz)$ was taken as a basis for the more realistic model [14] used in the present method. The applications of the method presented in this work do not include fluorescence enhancements, since it is negligible in the cases studied. For the sake of simplicity, the examples presented here deal with $\gamma Q_{j,q} \omega_{j,q}$ as a global scale factor for each L-subshell.

The actual registered spectrum involves not only the emitted bremsstrahlung and characteristic lines, but also different features of the detection system. In the case of lithium-drifted silicon detectors, Si(Li), like those used in this work, a linear calibration is implemented by means of two parameters, namely the *gain* factor and the *zero* shift, which depend on the detection chain settings. On the other hand, the detector system response for photons of energy E is a more or less broadened peak, whose distribution can be considered as Gaussian to a first approximation, its standard deviation σ being a function of photon energy [15]:

$$\sigma = (n^2 + \varepsilon F E)^{1/2} \quad (4)$$

where n is the uncertainty due to the electronic noise of the amplification process, F is the Fano factor and ε is the mean energy required for a single electron-hole pair formation −3.76 eV in Si(Li) detectors at 77 K.

Although the detector efficiency is close to 100% above 3 keV, it falls at lower energies owing to absorption in the front window and layers. The POEMA code is able to refine the three thicknesses characterizing the detector efficiency: the isolating window (beryllium, in the instrument used), the contact layer evaporated onto the front surface (gold, in the present situation), and the dead silicon layer.

The code POEMA can deal with some other artifacts. For example, the spurious Si peak due to the photoelectric absorption of a photon within the dead Si layer of the detector. Another effect taken into account is due to the fact that some of the charge carriers produced by a photon arriving at the detector may be trapped before being collected, resulting in registered energies lower than the original one. This is manifested in asymmetrical peaks with low energy tails, which become more evident for soft X-rays, since the highest concentration of traps occurs in a transient region close to the detector surface (between the active volume and the dead layer). In order to account for this effect, a modification to the Gaussian function has been included in POEMA by means of the Hypermet function: [16]

$$H_{j,q}(E_i) = M[G_{j,q}(E_i) + S_{j,q}(E_i) + T_{j,q}(E_i)]$$

where M is a normalization factor, $G_{j,q}(E_i)$ is a Gaussian function centered at the characteristic energy $E_{j,q}$:

$$G_{j,q}(E_i) = \frac{1}{\sqrt{2\pi}\ \sigma_{j,q}} \exp\left[-\frac{(E_i - E_{j,q})^2}{2\sigma_{j,q}^2} \right],$$

$S_{j,q}(E_i)$ is the step function of height $s_{j,q}$ convoluted by the Gaussian:

$$S_{j,q}(E_i) = s_{j,q}\mathrm{erfc}\left(\frac{E_i - E_{j,q}}{\sqrt{2}\sigma_{j,q}}\right)$$

and $T_{j,q}(E_i)$ is an exponential tail of width $\beta_{j,q}$ and height $t_{j,q}$ convoluted by the Gaussian:

$$T_{j,q}(E_i) = t_{j,q}e^{(E_i - E_{j,q})/\beta_{j,q}}\ \mathrm{erfc}\left(\frac{E_i - E_{j,q}}{\sqrt{2}\sigma_{j,q}} + \frac{\sigma_{j,q}}{\sqrt{2}\beta_{j,q}}\right)$$

In these functions, the parameters $s_{j,q}$, $t_{j,q}$ and $\beta_{j,q}$ are usually not known a priori and must be refined if peak asymmetries are taken into account.

At present, the code POEMA does not include escape and sum peaks, as far as they do not influence the parameters refined here. On the one hand, the escape peaks might become important only for low energies; on the other hand, sum peaks are important only for too high statistics, a situation avoided in the present work.

Bearing in mind the description given above, the intensity corresponding to the energy $E_i = zero + i \cdot gain$ for channel i may be predicted by:

$$\tilde{I}_i = B(E_i) + \sum_{j,q} P_{j,q}H_{j,q}(E_i) + P_{\mathrm{si}}G_{\mathrm{si}}(E_i)$$

where P_{Si} is the internal fluorescent Si peak, spread by means of a Gaussian distribution G_{Si}. The parameters which may be optimized in order to minimize the value of χ^2 of Eq. (1) are: the scaling factors α and the product $\gamma Q_{j,q}\omega_{j,q}$ of Eq. (2) and Eq. (3), the zero and gain of the detection chain, the peak-width factors n and F of Eq. (4), the transition rates $f_{j,q}$ and the mass concentrations C_j of Eq. (3), the three parameters involved in the function $H_{j,q}$ for each peak, the three thicknesses associated to the detector efficiency, the amplitude of the P_{Si} peak, the transition energies for the involved decays, etc.

Among the different numerical minimization routines (see, e.g. Ref. [17]) in the literature, the downhill simplex method [18] was chosen for POEMA because it is a robust algorithm and it requires only function evaluations, not derivatives, to carry out the refinement procedure. It is helpful to perform this process by choosing one or two parameters at a time; once convergence is achieved for them, they are set fixed and other reduced group of parameters is allowed to vary. When all the chosen parameters seem to have converged, the procedure should be restarted with the obtained values as initial guesses, moving all of them simultaneously. A particular feature related to the optimization of transition rates is the use of the normalization equation relating all the decays to the same atomic subshell at the end of each iteration, a process repeated until convergence. As an alternative to make an appropriate decision for the strategy to adopt during the optimization scheme, POEMA permits a visual examination of the intermediate results.

Once convergence is achieved, an estimate is given for the uncertainty of each parameter. To this end, the experimental spectrum is regarded as a vector **y** whose components are the number of counts at each channel. The parameters to optimize can be also thought as a vector **x**, and the function relating both, as a matrix $M(\mathbf{x})$. It can be seen [7] that the uncertainties of the parameters x_i, arising from the variance-covariance matrix V_x can be related to the variance-covariance matrix V_y for the experimental spectrum by means of:

$$V_x = [A^T(V_y)^{-1}A]^{-1}$$

where $A_{ij} = \partial M_i/\partial x_j$. The program performs these derivatives numerically in order to yield the matrix V_x, whose diagonal elements are the searched variances for each parameter x_i.

3. Results and discussion

In order to obtain values for L-subshell transition rates, several spectra of standard samples were used. These were acquired for pure samples in a JEOL JXA-733 at beam current values of 2 nA: Ta, Pt and W were measured at 30 keV during 500 s, whilst Pb and Bi were recorded at 38 keV and 400 s. In addition, for Ba transition rates a spectrum of $BaSO_4$ was measured in a scanning microscope JSM-840 with a beam current of 1.46 nA at 15 keV during 200 s. Both instruments are equipped with a Si(Li) detector attached to an energy-dispersive detection system.

The program developed allows to modify the input file, in order to choose the parameters to be optimized. As explained above, the best choice is to begin with the refinement of a few parameters;

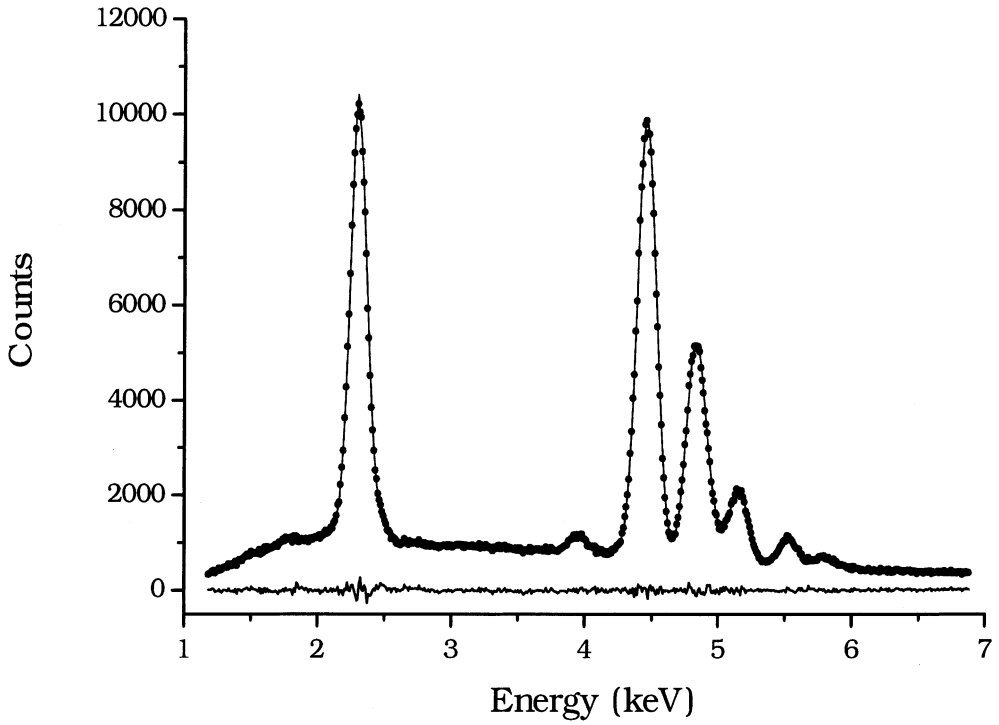

Fig. 1. Prediction for a $BaSO_4$ spectrum irradiated at 15 keV. Dots: experimental; solid curve: predicted spectrum; bottom curve: differences.

for the cases presented below, the first refinement is always performed on the overall scale factors α and the product $\gamma Q_{j,q}\omega_{j,q}$, using the data tabulated in the AXIL package [19] as initial estimates for the line transition rates. Typically, after this first step, an additional refinement of the calibration and detector response parameters is necessary.

In the present work, except for S, the asymmetry parameters were not obtained from the processed spectra, but from pure Ti (for Ba), Cu (for Ta, W and Pt) and Zr spectra (for Pb and Bi), since their spectra present few peaks. This equivalence is based on the fact that these K-lines are in the same energy region as the L-lines considered.

Regarding the detector efficiency, the three characteristic thicknesses are usually provided by the detector manufacturer, but their values may change with time due to different reasons. The beryllium window often becomes stained with oil molecules coming from the vacuum pump. In addition, the cooling system may favor the nucleation of water molecules, resulting in the growth of ice crystals on the gold surface layer. Finally, the dead silicon layer may be modified because of the migration of lithium atoms within the crystal. Bearing these ideas in mind, the corresponding effective thicknesses for the two detectors used were obtained by means of a procedure similar to that described in Bonetto et al. [8]

Once final convergence is achieved, the predicted spectra show a very good agreement with the experimental ones, as can be seen in the example shown in Fig. 1. In this case, corresponding to a $BaSO_4$ spectrum, $\chi^2 = 1.37$. The Fano factor obtained was 0.119 ± 0.004, in agreement with typical values [20]. The good performance achieved implies that the models used for the different processes involved are correct.

The transition rates for 14 to 20 different atomic decays (depending on the element) were obtained for Ba, Ta, W, Pt, Pb and Bi. The strategy followed

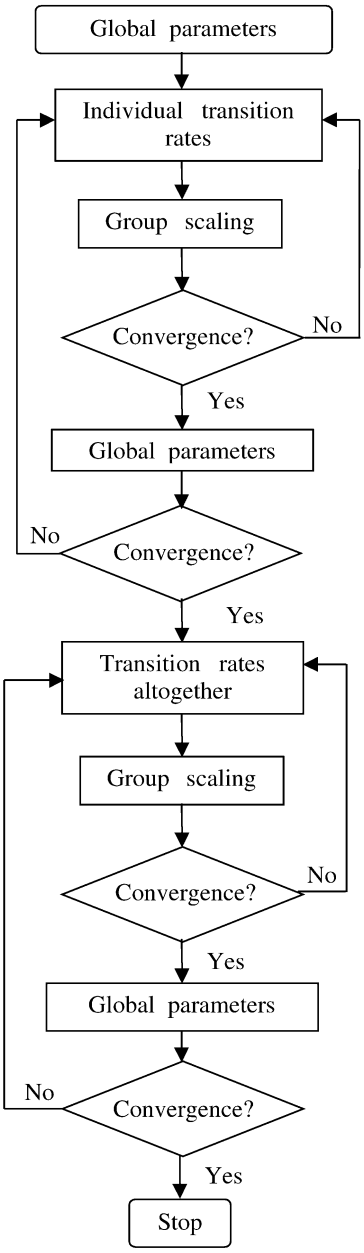

Fig. 2. Block diagram corresponding to the refinement strategy followed to obtain L-shell transition rates.

to obtain the final values is sketched in Fig. 2, where:

Global parameters: corresponds to the refinement of all the experimental and overall parameters involved in the optimization process, i.e. line group and background scale factors, calibration coefficients and detector system response parameters (noise and Fano factor).

Individual transition rates: points to the individual refinement of every single transition rate. In fact, for the cases where line energies are separated less than two times the detection system gain factor (40 eV/channel for all the elements except for $BaSO_4$ spectra, acquired with 10 eV/channel), peaks were grouped in one single step.

Group scaling: refers to optimize the different scale factors for each line group.

Convergence: is achieved when χ^2 repeats at least three significative digits from the previous refining step.

Transition rates altogether: stands for the refinement of all transition rates in one single optimization stage (leaving at least one free line ratio for each group, in order to fulfill the normalization condition).

The data obtained are displayed in column 2 of Tables 1–6. Those transition rates for which uncertainties were above 50% were excluded from the tables: these data correspond to very weak lines and their determination should be carried out by means of a spectrometer with better resolution (e.g. a wavelength dispersive system). Tables also show experimental data compiled by CRC Press in 1994 [3], theoretical values calculated by Scofield [1] and tabulated data from the Evaluated Atomic Data Library (EADL) by the Lawrence Livermore National Laboratory [2]. As can be seen from these tables, some of the obtained transition rates lack of uncertainty estimations. These cases correspond to very weak lines that could not be optimized; their values were obtained just from the normalization condition.

Regarding the precision of the values achieved, approximately 82% of them exhibit uncertainties lower than 10% or within the dispersion of the data given by other authors (provided that more than one is available). On the other hand, considering the accuracy of the results, in 75% of the cases, the values obtained are indistinguishable of any of the tabulated ones, or they do not fall apart from them more than the discrepancy found in the

Table 1
Transition rates for Ba L-shell (in $BaSO_4$)

Transition	This work	Ref. [3] CRC	Scofield [1]	Perkins et al. [2]
α_1 L_3M_5	0.714±0.012	0.736	0.737	0.711
α_2 L_3M_4	0.111±0.012	0.082	0.083	0.080
$\beta_{2,15}$ $L_3N_{4,5}$	0.1354±0.0024	0.1522	0.1400	0.1251
ℓ L_3M_1	0.0301±0.0009	0.0296	0.0317	0.0739
β_6 L_3N_1	0.0084±0.0011	–	0.0072	0.0071
$\beta_7L_3O_1$	0.0014	–	0.0013	0.0011
β_1 L_2M_4	0.8425±0.0042	0.8522	0.8271	0.8192
γ_1 L_2N_4	0.1351±0.0022	0.1236	0.1440	0.1323
η L_2M_1	0.0220±0.0029	0.0243	0.0233	0.0408
β_3 L_1M_3	0.463±0.011	0.545	0.466	0.474
β_4 L_1M_2	0.307±0.013	0.324	0.300	0.306
$\gamma_{2,3}$ $L_1N_{2,3}$	0.1894±0.0059	–	0.1808	0.1788
γ_4 $L_1O_{2,3}$	0.0295±0.0051	–	0.0301	0.0263
β_9 L_1M_5	0.0163	–	–	0.0074

literature (again, provided that more than one source are available).

Some of the lines studied here present overlapping effects. This problem, usual in EDS, remains even when the system gain factor is reduced—within the possibilities of the technique. Among the transition rates analyzed in this work, this inconvenience arises in eleven line groups: eight of them have been adequately managed by the POEMA program (e.g. Ta-Lα group); in two line-pairs, the program properly fits one line of each group (e.g. Ba-Lα_1 from the Ba-Lα group); finally, in only one case (Pt-Lα group), both lines were not accurately optimized. It is worth emphasizing that, in spite of the inherent limitations of an EDS, most of these severe overlapping effects were solved by means of the refinement method used here.

Table 2
Transition rates for Ta L-shell

Transition	This work	Scofield [1]	Perkins et al. [2]
α_1 L_3M_5	0.7160±0.0025	0.7175	0.7165
α_2 L_3M_4	0.0804±0.0022	0.0815	0.0812
$\beta_{2,15}$ $L_3N_{4,5}$	0.1509±0.0008	0.1489	0.1398
ℓ L_3M_1	0.0342±0.0006	0.0370	0.0483
β_6 L_3N_1	0.0133±0.0053	0.0089	0.0088
β_5 $L_3O_{4,5}$	0.0034	0.0032	0.0025
β_1 L_2M_4	0.804±0.012	0.8087	0.816
γ_1 L_2N_4	0.1547±0.0013	0.1582	0.1501
η L_2M_1	0.0310±0.0011	0.0233	
γ_5 L_2N_1	0.0032±0.0009	0.0055	0.0055
γ_6 L_2O_4	0.0052±0.0010	0.0036	0.0028
γ_8 L_2O_1	0.0008	0.0009	0.0010
β_{17} L_2M_3	0.0013	–	0.0007
β_3 L_1M_3	0.4145±0.0062	0.4123	0.415
β_4 L_1M_2	0.3249±0.0090	0.3228	0.326
γ_3 L_1N_3	0.1045±0.0068	0.1096	0.1069
γ_2 L_1N_2	0.0966±0.0069	0.0807	0.0796
γ_4 $L_1O_{2,3}$	0.0274±0.0030	0.0286	0.0273
β_9 L_1M_5	0.0162	–	0.0138
β_{10} L_1M_4	0.0110	–	0.0092

Table 3
Transition rates for W L-shell

Transition	This work	Ref.[3] CRC	Perkins et al.[2]
α_1 L_3M_5	0.7060±0.0041	0.7122	0.7146
α_2 L_3M_4	0.0851±0.0035	0.0795	0.0810
$\beta_{2,15}$ $L_3N_{4,5}$	0.1570±0.0015	0.1619	0.1409
ℓ L_3M_1	0.0366±0.0010	0.0339	0.0477
β_7 L_3N_1	0.0016	–	0.0018
β_5 $L_3O_{4,5}$	0.0056	0.0036	0.0037
β_1 L_2M_4	0.795±0.010	0.8222	0.8136
γ_1 L_2N_4	0.1521±0.0022	0.1546	0.1514
η L_2M_1	0.0329±0.0019	0.0173	0.0230
γ_5 L_2N_1	0.0074±0.0015	–	0.0055
β_17 L_2M_3	0.0076±0.0017	–	0.0007
β_3 L_1M_3	0.384±0.012	0.4462	0.410
β_4 L_1M_2	0.347±0.018	0.3146	0.328
γ_3 L_1N_3	0.086±0.027	0.1419	0.107
γ_2 L_1N_2	0.116±0.053	0.0973	0.080
γ_4 $L_1O_{2,3}$	0.0341±0.0053	–	0.0285
β_9 L_1M_5	0.0158	–	0.0142
β_{10} L_1M_4	0.0104	–	0.0095

Table 4
Transition rates for Pt L-shell

Transition	This work	Ref. [3] CRC	Perkins et al. [2]
α_1 L_3M_5	0.7180 ± 0.0030	0.6958	0.7051
α_2 L_3M_4	0.0635 ± 0.0023	0.0777	0.0800
$\beta_{2,15}$ $L_3N_{4,5}$	0.1524 ± 0.0012	0.1670	0.1449
ℓ L_3M_1	0.0369 ± 0.0008	0.0358	0.0461
β_6 L_3N_1	0.0098 ± 0.0008	0.0100	0.0095
β_7 L_3O_1	0.0078 ± 0.0010	–	0.0020
β_5 $L_3O_{4,5}$	0.0116 ± 0.0009	0.0138	0.0107
β_1 L_2M_4	0.7836 ± 0.0040	0.8044	0.8014
γ_0 L_2N_4	0.1618 ± 0.0022	0.1587	0.1564
η L_2M_1	0.0243 ± 0.0017	0.0175	0.0218
γ_5 L_2N_1	0.0077 ± 0.0015	–	0.0055
γ_6 L_2O_4	0.0142 ± 0.0016	0.0193	0.0122
γ_8 L_2O_1	0.0047 ± 0.0018	–	0.0011
β_{17} L_2M_3	0.0037 ± 0.0016	–	0.0008
β_3 L_1M_3	0.400 ± 0.016	0.426	0.390
β_4 L_1M_2	0.3376 ± 0.0094	0.3258	0.3325
γ_3 L_1N_3	0.1075 ± 0.0083	0.1440	0.1054
γ_2 L_1N_2	0.0871 ± 0.0070	0.1043	0.0836
γ_4 $L_1O_{2,3}$	0.0347 ± 0.0062	–	0.0324
β_9 L_1M_5	0.0166 ± 0.0064	–	0.0162

3.1. An application to quantitative analysis

Although quantitation methods involving the use of standards give usually more accurate compositions, standardless methods are often the only alternative to obtain analytical results, since a complete and adequate set of standards is not always available for the analyst. Due to the fact that the spectral prediction used in POEMA involves mass concentrations as parameters, it can be used as a standardless quantitation tool. Up to now, examples involving only K lines were faced

Table 5
Transition rates for Pb L-shell

Transition	This work	Ref. [3] CRC	Scofield [1]	Perkins et al. [2]
α_1 L_3M_5	0.6992 ± 0.0027	0.6833	0.6909	0.6951
α_2 L_3M_4	0.0682 ± 0.0020	0.0763	0.0786	0.0790
$\beta_{2,15}$ $L_3N_{4,5}$	0.156 ± 0.010	0.1697	0.1554	0.1486
ℓ L_3M_1	0.0401 ± 0.0008	0.0381	0.0406	0.0451
β_6 L_3N_1	0.0114 ± 0.0006	0.0107	0.0102	0.0101
β_7 L_3O_1	0.0036 ± 0.0016	–	0.0021	0.0022
β_5 $L_3O_{4,5}$	0.0213 ± 0.0009	0.0219	0.0203	0.0177
β_1 L_2M_4	0.7937 ± 0.0049	0.7881	0.7796	0.7888
γ_1 L_2N_4	0.1658 ± 0.0024	0.1650	0.1674	0.1611
η L_2M_1	0.0244 ± 0.0019	0.0181	0.0215	0.0215
γ_5 L_2N_1	0.0036 ± 0.0016	–	0.0056	0.0055
β_8 L_2O_1	0.0012	–	0.0012	0.0012
β_{17} L_2M_3	0.0009	–	–	0.0009
β_3 L_1M_3	0.4224 ± 0.0024	0.4019	0.3660	0.3683
β_4 L_1M_2	0.3507 ± 0.0095	0.3384	0.3334	0.3372
γ_3 L_1N_3	0.112 ± 0.046	0.145	0.107	0.103
γ_2 L_1N_2	0.109 ± 0.025	0.115	0.088	0.087

Table 6
Transition rates for Bi L-shell

Transition	This work	Perkins et al. [2]
α_1 L_3M_5	0.6902 ± 0.0027	0.6929
α_2 L_3M_4	0.0755 ± 0.0019	0.0787
β_2 L_3N_5	0.1414 ± 0.0068	0.1345
β_{15} L_3N_4	0.0159 ± 0.0064	0.0149
ℓ L_3M_1	0.0412 ± 0.0009	0.0450
β_6 L_3N_1	0.0115 ± 0.0007	0.0103
β_5 $L_3O_{4,5}$	0.0227 ± 0.0010	0.0193
$\beta 1$ L_2M_4	0.7891 ± 0.0050	0.7859
γ_1 L_2N_4	0.1631 ± 0.0024	0.1623
η L_2M_1	0.0264 ± 0.0019	0.0214
γ_8 L_2O_1	0.0012	0.0012
β_{17} L_2M_3	0.0009	0.0009
β_3 L_1M_3	0.428 ± 0.048	0.374
β_4 L_1M_2	0.365 ± 0.010	0.350
γ_2 L_1N_2	0.102 ± 0.020	0.090

[8]. An interesting test is to carry out an analytical procedure by using the values for L transition rates obtained in the previous section. The example shown here involves a benitoite sample ($BaTiSi_3O_9$), measured in the JSM-840 microscope with a beam current of 1.47 nA at 15 keV during 200 s. This sample has been deliberately chosen because of the strong overlapping of Ba-L and Ti-K lines. The results obtained here are compared in Table 7 to those given by the peak-to-background (P/B) standardless algorithm [12] included in MULTI package [21].

For this application of POEMA, the mass concentrations were refined using the output produced by MULTI-P/B as initial guesses. For the scale factors and the detection system calibration and response parameters, the values obtained from the $BaSO_4$ sample were used as starting estimates. In the first optimization step, the calibration, detection system response and background scale parameters were refined. During the refinement process, the ratios between the different scale factors were maintained fixed, although they were allowed to vary altogether.

Once convergence was achieved for these parameters, mass concentrations were refined for all the elements with the exception of oxygen. Since this element is not detectable with the conventional equipment used, its concentration was obtained like in MULTI as $3A_O/A_{Si}$ times the silicon mass concentration—where A stands for atomic weight. The following step is to normalize concentrations to 100%. Afterwards, the whole cycle is repeated up to final convergence. As can be seen from Table 7, the concentration values refined by POEMA are quite better than those produced by MULTI-P/B. Moreover, Table [7] also evidences that the results obtained are almost as good as those produced by another quantitation method (MULTI-S), which requires the corresponding information from adequate standards. The algorithm used for these assessments is based on the Gaussian depth distribution function modeled by Riveros et al. [14], which is also included in MULTI.

4. Conclusions

The capability of program POEMA for the refinement of L-shell transition rates has been shown for 104 decays corresponding to six different elements. Even when the energy detection system gain factor was rather large, the results obtained are very good in view of the scarce updated experimental data and highly scattered theoretical values for L line-ratios appearing in the literature. The optimization method may be extended to wavelength dispersive spectrometers, by performing some modifications related to specific characteristics of the detection system. This allows the spectra to be studied with better resolution, which implies results with lower uncertainties.

In addition, an example of the optimization procedure as a quantitation tool has been shown for a sample which exhibits L-lines strongly, overlapped with K lines, a problem usually difficult for the analyst to solve. The results are actual improvements for the mass concentrations pro-

Table 7
Mass concentrations predicted by POEMA as compared to two quantitation algorithms and the certified values for a benitoite sample

Element	This work	MULTI-P/B	MULTI-S	Nominal
Si	0.2049 ± 0.0010	0.2516	0.2019	0.2038
Ti	0.0994 ± 0.0010	0.1064	0.1311	0.1159
Ba	0.3515 ± 0.0018	0.2370	0.3220	0.3322
O	0.3463 ± 0.0014	0.4050	0.3450	0.3481

duced by another standardless algorithm, and they are similar to those obtained by a conventional quantitation method involving standards.

Acknowledgments

This work was partially supported by the Consejo Nacional de Investigaciones Científicas y Técnicas de la República Argentina, the Agencia Córdoba Ciencia and the Secretaría de Ciencia y Técnica de la Universidad Nacional de Córdoba, Argentina.

References

[1] J.H. Scofield, Hartree-Fock values of L X-ray emission rates, Phys. Rev. A 10 (1974) 1507-1510 [Erratum: Phys. Rev. A 12 (1975) 345].
[2] S.T. Perkins, D.E. Cullen, M.H. Chen, J.H. Hubbell, J. Rathkopf, J. Scofield, Tables and graphs of atomic subshells and relaxation data derived from LLNL evaluated atomic data library (EADL), Z = 1–100, Lawrence Livermore National Laboratory, Report UCRL-50400, vol. 30, 1991.
[3] Handbook of Chemistry and Physics, CRC Press, BocaRaton; D.R. Lide, ed., 74th edition, 1994.
[4] H.M. Rietveld, The crystal structure of some alkaline earth metal uranates of the type M_3UO_6, Acta Cryst. 20 (1966) 508–513.
[5] H.M. Rietveld, Line profiles of neutron powder-diffraction peaks for structure refinement, Acta Cryst. 22 (1967) 151–152.
[6] H.M. Rietveld, A profile refinement method for nuclear and magnetic structures, J. Appl. Cryst. 2 (1969) 65–71.
[7] R.A. Young, The Rietveld Method, International Union of Crystallography, Oxford University Press, Oxford, 1993.
[8] R. Bonetto, G. Castellano, J. Trincavelli, Optimization of parameters in electron probe microanalysis, X-Ray Spectrom. 30 (2001) 313–319.
[9] G. Castellano, R. Bonetto, J. Trincavelli, M. Vasconcellos, C. Campos, Optimization of K-shell intensity ratios in electron probe microanalysis, X-Ray Spectrom. 31 (2002) 184–187.
[10] A. Carreras, R. Bonetto, G. Stutz, J. Trincavelli, G. Castellano, Parameter refinement in the analysis of X-ray irradiated samples, X-Ray Spectrom. 31 (2002) 173–177.
[11] J. Trincavelli, G. Castellano, J.A. Riveros, X-Ray Spectrom. 27 (1998) 81–86.
[12] J. Trincavelli, R. Van Grieken, X-Ray Spectrom. 23 (1994) 254–260.
[13] R.H. Packwood, J.D. Brown, X-Ray Spectrom. 10 (1981) 138–145.
[14] J.A. Riveros, G. Castellano, J. Trincavelli, Mikrochim. Acta 12 (1992) 99–105, [Suppl.].
[15] J.I. Goldstein, D.E. Newbury, P. Echlin, D.C. Joy, A.D. Romig, C.E. Lyman, C.E. Fiori, E. Lifshin, Scanning Electron Microscopy and X-Ray Microanalysis, 2nd ed, Plenum Press, New York, 1992, p. 311.
[16] G.W. Phillips, K.W. Marlow, Authomatic analysis of gamma-ray spectra from germanium detectors, Nucl. Instrum. Methods 137 (1976) 525–536.
[17] W.H. Press, B.P. Flannery, S.A. Teukolsky, W.T. Vetterling, Numerical Recipes, Cambridge University Press, Cambridge, 1989.
[18] J.A. Nelder, R. Mead, A simplex method for function minimization, Comput. J. 7 (1965) 308–313.
[19] P. Van Espen, K. Janssens, J. Nobels, AXIL-PC software for the analysis of complex X-ray spectra, Chemom. Intell. Lab. Syst. 1 (1987) 109–114.
[20] G.F. Knoll, Radiation Detection and Measurement, 2nd. ed., John Wiley and Sons, New York, 1989.
[21] J. Trincavelli, G. Castellano, MULTI: an interactive program for quantitation in EPMA, X-Ray Spectrom. 28 (1999) 194–197.